Evaluation of thin-film nanocomposite RO membranes using TiO$_2$ nanotubes and TiO$_2$ nanoparticles: a comparative study

Jungchan Kim, Youngbin Baek, Sung Pil Hong, Hongsik Yoon, Seonghwan Kim, Choonsoo Kim, Jiye Kim, Jeyong Yoon*

School of Chemical and Biological Engineering, Institute of Chemical Process, Asian Institute for Energy, Environment and Sustainability (AIEES), Seoul National University, Daehak-dong, Gwanak-gu, Seoul 08826, Korea, Tel. +82 2 880 8941; Fax: +82 2 876 8911; emails: jungchani@snu.ac.kr (J. Kim), ybbaek@snu.ac.kr (Y. Baek), dhaos86@snu.ac.kr (S.P. Hong), hongsik07@snu.ac.kr (H. Yoon), nakshia@snu.ac.kr (S. Kim), genius21@snu.ac.kr (C. Kim), imkjy5@snu.ac.kr (J. Kim), jeyong@snu.ac.kr (J. Yoon)

ABSTRACT

Thin-film nanocomposite (TFN) reverse osmosis (RO) membranes have gained attention due to their enhanced membrane performances in permeate flux and salt rejection. The structural shape of nanocomposites, such as particles and nanotubes, has been thought to have critical roles in improving their performances. However, the effects of the structural properties on membrane performance have yet to be verified. Herein, we reported the structural effects of nanocomposites on the performance of TFN RO membranes fabricated with TiO$_2$ nanotubes (TNT) and TiO$_2$ nanoparticles (TNP). The TFN RO membranes containing TNT or TNP exhibited similar high hydrophilicities and enhanced water permeability compared with a conventional RO membrane. In terms of membrane performance, the TNT TFN RO membranes had better water permeability than the TNP TFN RO membranes. Compared with non-porous TNP, 80-nm diameter nanochannels of TNT provided additional enhanced water permeability by serving as water transport passageways.

Keywords: TiO$_2$ nanotube; TiO$_2$ nanoparticle; Thin-film nanocomposite RO membrane; Permeate flux

1. Introduction

Reverse osmosis (RO) has been widely used in desalination processes and requires relatively low energy consumption [1]. Currently, polyamide (PA) thin-film composite (TFC) RO membranes comprise over 90% of the market for RO membranes due to their high water permeability and high selectivity [2]. Along with the wide applicability of PA TFC RO membranes, efforts are being made to reduce the energy consumption of the RO process to produce water at lower costs [3]. To this end, various nanomaterials have been used to improve membrane performance [4]. Thin-film nanocomposite (TFN) RO

*Corresponding author.

membranes, fabricated by embedding nanomaterials in polymeric selective layers (e.g. PA), have been developed to improve the performance of RO membranes, including increasing permeate flux and antifouling properties [5]. These improvements depend on the characteristics of the embedded nanomaterials [6].

Table 1 summarizes the various nanomaterials that have been used as embedded materials and their corresponding effects on TFN RO membranes. The nanomaterials can be classified as nanoparticles (e.g. TiO_2, zeolites, SiO_2, and Ag) and nanotubes (e.g. carbon nanotubes (CNTs) and TiO_2 nanotubes (TNTs)). In terms of nanoparticles, Jeong et al. [7] first reported embedding zeolite A into a PA layer. This zeolite A PA TFN RO membrane showed an approximately 80% enhanced permeate flux and maintained a high level of salt rejection. Similarly, $PA-TiO_2$ nanocomposite membranes displayed a 95% rejection of $MgSO_4$ and a 9.1 LMH permeate flux, i.e. levels higher than those of PA TFC membranes [8]. SiO_2 and Ag nanoparticle-based TFN RO membranes also showed enhanced permeate flux [9,10]. Furthermore, nanotube-based TFN RO membranes exhibited superior performance compared with PA TFC RO membranes. For example, a TNT TFN RO membrane was synthesized by a hydrothermal method using silane-coupled, amino-functionalized TiO_2 nanoparticles [11]. This TNT TFN RO membrane showed an approximately 93% enhanced water permeability and an anti-organic fouling property. In the same manner, a CNT TFN RO membrane, which was fabricated by the deposition of oxidized CNTs on a PA layer covered with polyvinyl alcohol, showed an approximate 30% enhanced permeate flux while maintaining salt rejection [12].

These enhanced membrane performances can be explained in two ways. First, the increased hydrophilicity on the membrane surface was due to the embedded hydrophilic nanomaterials, including pre-treated CNTs [7,9,10,13,16,17]. Second, the inner void spaces of nanotubes [14–16,18,19] or gaps between the polyamide layers and nanomaterials provided for fast diffusion rates [15,17,20]. However, the effects of structural properties on membrane performance have yet to be verified. Furthermore, the effects of the embedded nanomaterials and their hydrophilic and void space contributions on performance enhancement in TFN RO membranes have to be identified. Most studies have only evaluated the performances of TFN RO membranes relative to those of TFC RO membranes; comparative studies between nanotube-based TFN RO membranes and nanoparticle-based TFN RO membranes have not been conducted.

The aim of this study was to compare the effect of embedded nanomaterials on TFN RO membrane using TNT and TNP, which are same materials that have different structure. Using a same material, both the TNT and TNP TFN RO membranes might have similar hydrophilicity which could independently evaluate the effect of the nanomaterial structure on the performance of the TFN RO membrane. TNT was synthesized via the anodic oxidation of Ti foil, and TNP was supplied from a commercial source. The morphology of the TNT and TNP structures was analyzed by SEM and TEM. The TNT and TNP TFN RO membranes were fabricated by interfacial polymerization. The surface properties of these TFN RO membranes were analyzed by SEM, EDS, and contact angle measurement. Permeate flux and salt rejection were measured in a lab scale cross-flow RO filtration system.

Table 1
Summary of various nanomaterials as embedded materials and their effects on membrane performance for TFN RO membranes

Nanomaterial		Permeate flux enhancement percentage (LMH)[a]	Refs.
Nanoparticle	Zeolite A	80% (17)	[7]
	TiO_2	35% (23)	[13]
	SiO_2	64% (47)	[9]
	Ag	24% (31)	[10]
Nanotube	TiO_2	93% (37)	[11]
	Carbon nanotubes	32% (51)	[14]
		27% (44)	[12]
		319% (29)	[15]

[a]Reported permeate flux.

2. Materials and methods

2.1. Synthesis of TiO$_2$ nanotube (TNT)

A TiO$_2$ nanotube (TNT) array was synthesized in an electrochemical cell consisting of a 2×3 cm Ti foil (Sigma–Aldrich) as an anode, a 2×3 cm Pt foil (Sigma–Aldrich) as a cathode, and an ethylene glycol solution containing 2.5 wt.% H$_2$O and 0.2 wt.% NH$_4$F (Sigma–Aldrich) as an electrolyte. The voltage was provided by a DC power supply (UDP-150I, Unicorn Tech Co., Korea). After anodization, the TNT array was annealed at 450℃ for 1 h under atmospheric pressure and detached from the Ti foil. Additional details on the synthesis of the TNT array were described in our previous report [21].

2.2. Characterization of TNT and TNP

The TNT array was analyzed by a field emission scanning electron microscope (FE-SEM; JSM-6701F, JEOL, Japan). The as-grown TNT array was cut into a 3×3 mm sample size and attached on carbon tape. The specimen was washed with ethanol and dried at room temperature.

The morphologies of TNT and TNP were observed by transmission electron microscope (TEM, Libra 120, Carl Zeiss). TiO$_2$ nanoparticles (TNPs; Aeroxide® P-25) were purchased from Evonik. The TNT array was dispersed in n-hexane (Sigma–Aldrich) using an ultrasonic bath (UCP-10, Jeio Tech Co., Korea) for 1 h and a tip-type sonicator (VCX500, Sonics and Materials, Inc., USA) for 10 min, consecutively. A 0.02 wt.% TNT solution and a 0.02 wt.% TNP solution in n-hexane were prepared. A few drops of each suspension were deposited onto 3-mm diameter carbon-coated grids. The TEM analyses were conducted at 120 kV acceleration voltage.

2.3. Fabrication of TNT TFN RO membrane and TNP TFN RO membrane

Fig. 1 describes the synthesis procedure of the TNT and TNP TFN RO membranes. First, a polysulfone (PSf) support membrane was prepared by phase inversion with 20 wt.% PSf (Mw 22,000 Da, Sigma–Aldrich) in N-methyl-2-pyrrolidinone (Sigma–Aldrich) and stabilized in deionized (DI; Millipore) water for 4 h. The PSf support membrane was positioned on a stainless plate with aluminum tape and soaked in a 2 wt.% m-phenylenediamine (MPD; >99%, Sigma–Aldrich) aqueous solution for 1 h. Excess MPD aqueous solution was removed using a rubber roller. The MPD-saturated PSf membrane was reacted with a 0.1 wt.% trimesoyl chloride (TMC; >98.5%, Sigma–Aldrich) solution in n-hexane for 1 min. The TMC solution was prepared by dispersing 0.01 and 0.02 wt.% TNT and 0.02 wt.% TNP by sonication (as mentioned in Section 2.1). These fabricated membranes were rinsed with n-hexane and cured in a dry oven at 75℃ for 4 min. A PA TFC RO membrane was synthesized by the same procedure without adding the nanomaterials in the TMC solution. The fabricated RO membranes were identified as TFC, TNT0.01, and TNT0.02 and TNP0.02. TFC, TNT, and TNP, respectively, indicate a plain PA RO membrane, a TNT TFN RO membrane, and a TNP TFN RO membrane; the numbers indicate the embedded nanomaterial weight percentages.
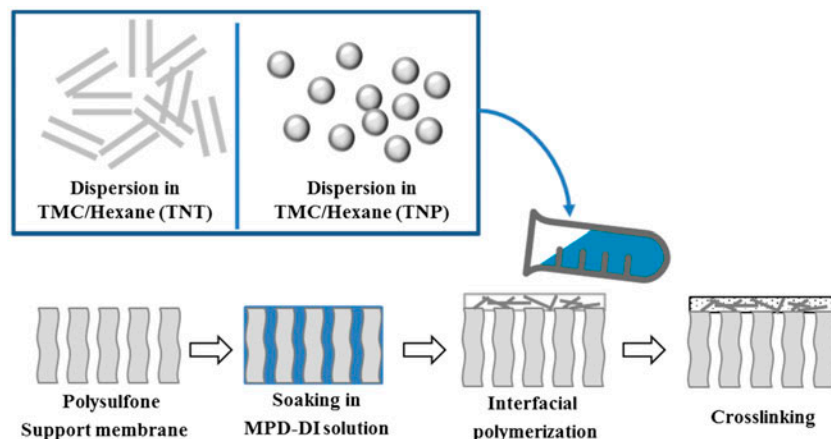
Fig. 1. Schematic of the interfacial polymerization procedure for fabrication of the TFN RO membrane using TiO$_2$ nanotube (TNT) or TiO$_2$ nanoparticle (TNP).

2.4. Characterization of TNT TFN RO membrane and TNP TFN RO membrane

The surface morphologies of the TNT and TNP TFN RO membranes were analyzed by FE-SEM. The membrane surface conductivity was enhanced by Pt sputtering at 10 mA for 120 s. Energy dispersive spectroscopy (EDS, JSM-6701F, JEOL, Japan) was used to detect the titanium in PA layer at 20 kV acceleration voltage. The membrane surface hydrophilicity was analyzed by a contact angle analyzer (DSA100, KRÜSS, Germany) using the captive bubble method [22]. Briefly, membrane samples were attached to a glass support and immersed in DI water at room temperature. Ten microliters of an air bubble droplet were formed at the end of a "J"-shaped syringe needle and slightly attached onto the membrane surface. At least five measurements were made for reproducibility and the average value with standard deviation was reported for each sample.

2.5. Membrane performance test

Membrane performances, such as permeate flux and salt rejection, were measured in a lab scale cross-flow filtration system [23]. The system consisted of a 6-L feed water tank and a membrane cell with a 22.4 cm^2 (3.3 × 6.8 cm) effective membrane area and 0.3-cm channel height. For membrane performance tests, 2,000 mg/L NaCl solution was fed into the system at a 7 cm/s cross-flow velocity at 30℃. After membrane compaction for 30 min at 15.5 bar, the permeate flux was measured under the same pressure by maintaining the permeate weight for 20 min. Permeate flux (J_w) was calculated by Eq. (1):

$$J_w = \frac{V}{a \times t} \tag{1}$$

where J_w is the permeate flux (LMH, L m^{-2} h^{-1}), V is the permeate volume (L), a is the effective membrane area (m^2), and t is the operation time (h).

Salt rejection (R_s) was evaluated by measuring the conductivity difference between the feed water and the permeate (Eq. (2)):

$$R_s = \left[1 - \frac{C_p}{C_f} \right] \times 100 \tag{2}$$

where R_s is the percentage ratio of the NaCl rejection, C_f is the conductivity of the feed water (mS/cm), and C_p is the conductivity of the permeate (mS/cm).

The water permeability (A; LMH/bar) and salt permeability (B; LMH) were calculated using Eqs. (3) and (4), respectively from the solution-diffusion model [24]:

$$A = J_w/\Delta P \tag{3}$$

where J_w is water flux and ΔP is the difference between hydraulic pressure and osmotic pressure (π).

$$B = J_s/(C_p - C_f) \tag{4}$$

where J_s is the salt flux attained by $J_w \times C_f$.
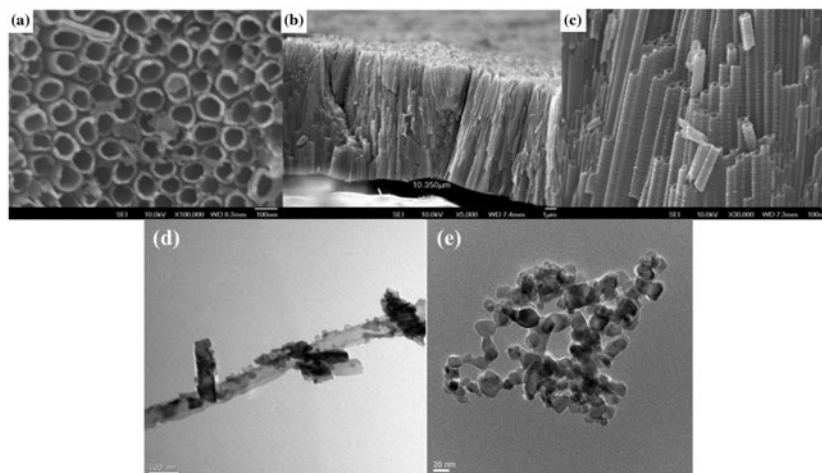
Fig. 2. SEM images of fabricated TNT array on Ti foil; (a) surface, (b) cross section, and (c) enlarged image of (b). TEM images of (d) TNT and (e) TNP.

3. Results and discussion

3.1. Characteristics of TNT and TNP

Figs. 2(a)–(c) show the SEM images of the fabricated TNT array. As shown in Fig. 2(a), the TNT array was densely packed and perpendicularly aligned on the Ti foil. The ends of the TNT array were opened, indicating that the shapes of individual TNTs were either round or oval and had pore sizes ranging from 70 to 80 nm with an approximately 10-nm-thick wall. In the cross section SEM image shown in Fig. 2(b), the average length of the TNT array was approximately 10 μm.

Figs. 2(d) and (e) show the TEM images of the morphology of the dispersed TNT and TNP, respectively. As shown in Fig. 2(d), the length of individual TNTs ranged from 0.1 to 1 μm, which was shorter than the average length of the TNT array (10 μm, Fig. 2(b)). The treatment of TNT by sonication likely separated individual TNTs from the TNT array and also shortened the length of the TNTs. The black particles in Fig. 2(d) may be broken residues of TNTs due to excessive sonication. However, the size of TNPs ranged from 10 to 50 nm, as shown in Fig. 2(e).

3.2. Characteristics of TNT TFN RO membrane and TNP TFN RO membrane

Fig. 3 shows the surface morphology of the TNT and TNP TFN RO membranes. Fig. 3(a), (b), and (c) present TNT0.02, TNP0.02, and TFC, respectively. As shown in Fig. 3(a), a cylindrically shaped TNT covered by a PA layer was observed on the TNT0.02 membrane. In the upper right corner of Fig. 3(b), well-dispersed TNPs were found on the surface of the TNP0.02 membrane, while the TFC membrane showed a typical surface morphology without any particles (Fig. 3(c)). The element weight percentage of the TNT0.02, TNP0.02, and TFC membranes was analyzed by energy dispersive spectroscopy (EDS; data not shown). Similar weight percentages of titanium were detected in the TNT PA TFN RO membrane (0.2 ± 0.1%) and the TNP TFN RO membrane (0.3 ± 0.1%), while the PA TFC RO membrane only presented carbon, oxygen, and sulfur.

The contact angles of TNT0.01 and TNT0.02, TNP0.02, and TFC are listed in Table 2. As shown in Table 2, the contact angle of TNT0.01 was 38.9°. TNT0.02 and TNP0.02 had the lowest contact angles (37.1° and 37.3°, respectively), while the TFC membrane showed the highest contact angle (45.9°). This result implied that the embedded TiO₂ nanomaterials modified the membrane surface property to be more
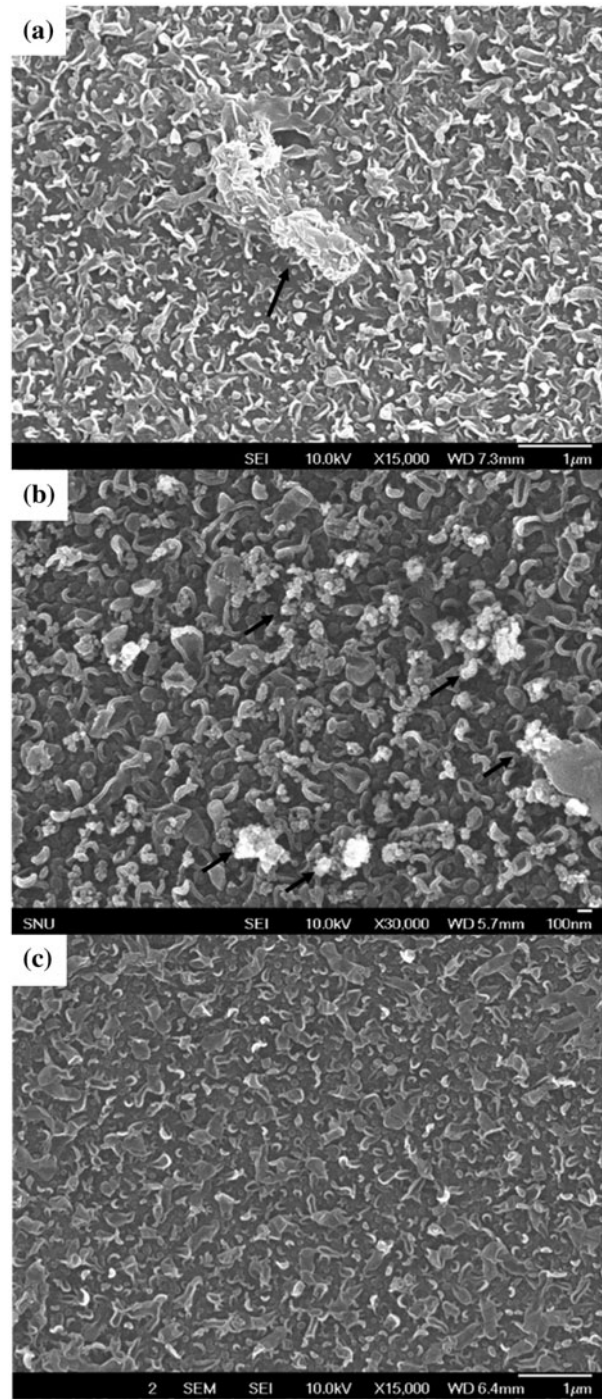
Fig. 3. Surface morphology of (a) 0.02 wt.% TNT TFN RO membrane, (b) 0.02 wt.% TNP TFN RO membrane, and (c) PA TFC RO membrane.

hydrophilic. This result was consistent with previous studies wherein hydrophilic nanomaterials, such as TiO₂ nanoparticle, zeolite A, and silver nanoparticle-

Table 2
Contact angles of TNT0.01, TNT0.02, TNP0.02, and TFC membranes

Membranes	Contact angle (°)[a]
TNT0.01	38.9 ± 1.3
TNT0.02	37.1 ± 1.2 (40)[b]
TNP0.02	37.3 ± 0.7
TFC	45.9 ± 1.0 (70)[b]

[a]Measured by captive bubble method [22].
[b]Sessile drop contact angle data from literature corresponding to TFN0.1 and TFC membranes [11].

embedded TFN RO membranes had more hydrophilic surfaces [7,10,25].

3.3. Performance of TNT TFN RO membrane and TNP TFN RO membrane

Fig. 4 illustrates the permeate flux and the salt rejection of the TNT0.01, TNT0.02, TNP0.02, and TFC membranes. As shown in Fig. 4, the permeate flux of TNT0.01 and TNT0.02 was enhanced to 43.0 and 54.7 LMH, respectively, as the amount of embedded TNT increased from 0.01 to 0.02 wt.% compared with the 37.0 LMH permeate flux of the PA TFC RO membrane. The TNP0.02 membrane showed a lower enhanced permeate flux (44.9 LMH) than that of the TNT0.02 membrane; however, the TNP0.02 membrane had a similar hydrophilicity. The salt rejection rates of the TNT0.01, TNT0.02, TNP0.02, and TFC membranes were 91.8, 92.6, 95.4, and 94.9%, respectively. As the TNT amount increased, the salt rejection slightly reduced for all membranes except TNP0.02.

Fig. 5 shows the correlations between the contact angle and the enhancements to water permeability
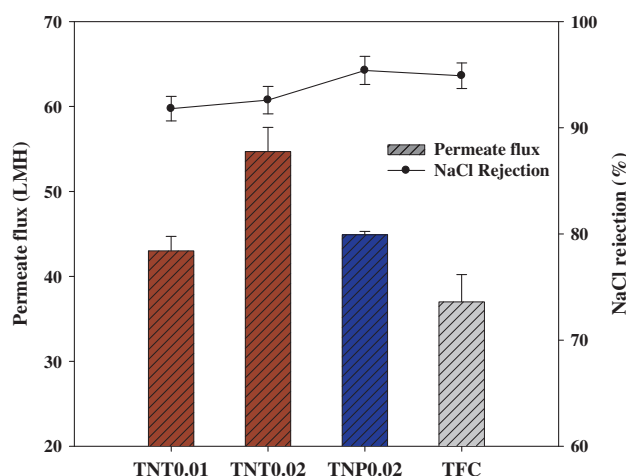
Fig. 4. Permeate flux and NaCl rejection of TNT0.01, TNT0.02, TNP0.02, and TFC membranes.

and salt permeability. As shown in Fig. 5, both water permeability and salt permeability were enhanced as the membrane surface became more hydrophilic. This improved hydrophilicity enhanced the permeate flux. This result was consistent with previous studies of TiO_2-based TFN RO membranes [8,16]. Interestingly, the TNP0.02 membrane (square) showed lower water and salt permeability enhancements than those of the TNT0.02 membrane. This indicated that the nanotube structure significantly enhanced the permeability, while the nanoparticle structure only slightly affected the permeability. The larger pore size of TNTs (approximately 80 nm) may have increased the sorption capacity of the RO membrane, which resulted in the greater permeability enhancement, whereas the TNP had no internal pores. This result correlated with the findings of a previous study of silica-based TFN RO
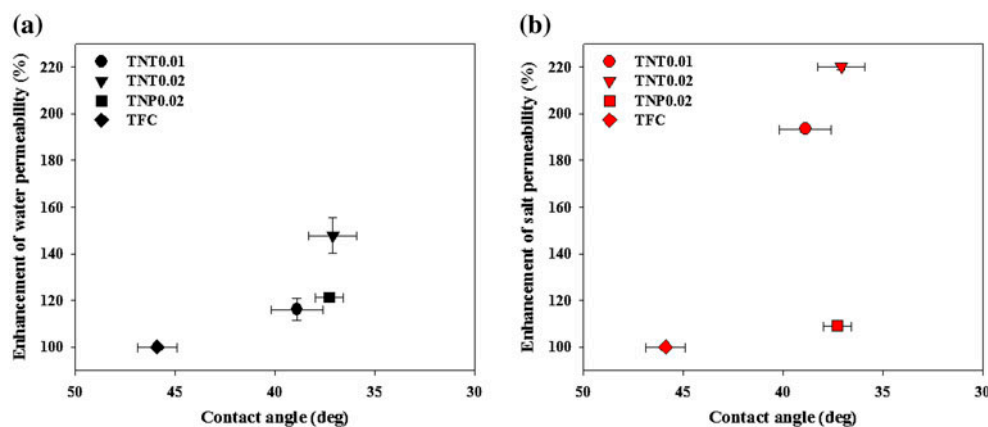
Fig. 5. Correlations between contact angle and (a) enhancement of water permeability and (b) enhancement of salt permeability.

membranes. In the past study, a non-porous silica-embedded TFN membrane showed 25% enhanced permeate flux, while a porous silica-embedded TFN membrane exhibited 64% enhanced permeate flux [9]. Moreover, the enhanced salt permeability was higher than that of water permeability in the TNT TFN RO membrane. As shown in Fig. 5(a) and (b), the water permeability of the TNT0.02 membrane increased by 48%, while the salt permeability increased by 120%. The larger pores of the TNTs contributed to higher salt and water permeability.

4. Conclusion

We compared the performances of TNT TFN RO membranes and TNP TFN RO membranes to evaluate the effect of embedded nanomaterials on TFN RO membranes. The hydrophilicity of the membrane surface was increased as the concentration of the TiO_2 nanomaterials increased in the TFN RO membranes, which resulted in high water and salt permeability. Under the same conditions, the TNT0.02 membrane showed a 48% higher water permeability and a 120% higher salt permeability than the TFC RO membrane, while the TNP0.02 membrane showed a 21% higher water permeability and a 9% higher salt permeability. These results indicated that the large pores (approximately 80 nm) of the TNTs significantly affected membrane permeability, whereas the TNPs, which had no pores but had a gap between the TNP and PA layers, only slightly affected membrane permeability. The permeability of TFN RO membranes could be affected by the hydrophilicity and the structure of embedded nanomaterials. Further studies are necessary to determine the effect of the size of embedded nanomaterials on membrane performance.

References

[1] M. Elimelech, W.A. Phillip, The future of seawater desalination: Energy, technology, and the environment, Science 333 (2011) 712–717.

[2] R.J. Petersen, Composite reverse osmosis and nanofiltration membranes, J. Membr. Sci. 83 (1993) 81–150.

[3] V.G. Gude, Energy consumption and recovery in reverse osmosis, Desalin. Water Treat. 36 (2011) 239–260.

[4] M.M. Pendergast, E.M. Hoek, A review of water treatment membrane nanotechnologies, Energy Environ. Sci. 4 (2011) 1946–1971.

[5] K.P. Lee, T.C. Arnot, D. Mattia, A review of reverse osmosis membrane materials for desalination—Development to date and future potential, J. Membr. Sci. 370 (2011) 1–22.

[6] W.J. Lau, S. Gray, T. Matsuura, D. Emadzadeh, J. Paul Chen, A.F. Ismail, A review on polyamide thin film nanocomposite (TFN) membranes: History, applications, challenges and approaches, Water Res. 80 (2015) 306–324.

[7] B.-H. Jeong, E.M.V. Hoek, Y. Yan, A. Subramani, X. Huang, G. Hurwitz, A.K. Ghosh, A. Jawor, Interfacial polymerization of thin film nanocomposites: A new concept for reverse osmosis membranes, J. Membr. Sci. 294 (2007) 1–7.

[8] H.S. Lee, S.J. Im, J.H. Kim, H.J. Kim, J.P. Kim, B.R. Min, Polyamide thin-film nanofiltration membranes containing TiO_2 nanoparticles, Desalination 219 (2008) 48–56.

[9] J. Yin, E.-S. Kim, J. Yang, B. Deng, Fabrication of a novel thin-film nanocomposite (TFN) membrane containing MCM-41 silica nanoparticles (NPs) for water purification, J. Membr. Sci. 423–424 (2012) 238–246.

[10] E.-S. Kim, G. Hwang, M. Gamal El-Din, Y. Liu, Development of nanosilver and multi-walled carbon nanotubes thin-film nanocomposite membrane for enhanced water treatment, J. Membr. Sci. 394–395 (2012) 37–48.

[11] D. Emadzadeh, W.J. Lau, M. Rahbari-Sisakht, A. Daneshfar, M. Ghanbari, A. Mayahi, T. Matsuura, A.F. Ismail, A novel thin film nanocomposite reverse osmosis membrane with superior anti-organic fouling affinity for water desalination, Desalination 368 (2015) 106–113.

[12] C. Kim, S. Kim, J. Choi, J. Lee, J.S. Kang, Y.E. Sung, J. Lee, W. Choi, J. Yoon, Blue TiO_2 nanotube array as an oxidant generating novel anode material fabricated by simple cathodic polarization, Electrochim. Acta 141 (2014) 113–119.

[13] H.S. Lee, S.J. Im, J.H. Kim, H.J. Kim, J.P. Kim, B.R. Min, Polyamide thin-film nanofiltration membranes containing TiO_2 nanoparticles, Desalination 219 (2008) 48–56.

[14] H.D. Lee, H.W. Kim, Y.H. Cho, H.B. Park, Experimental evidence of rapid water transport through carbon nanotubes embedded in polymeric desalination membranes, Small 10 (2014) 2653–2660.

[15] W.F. Chan, H.Y. Chen, A. Surapathi, M.G. Taylor, X.H. Shao, E. Marand, J.K. Johnson, Zwitterion functionalized carbon nanotube/polyamide nanocomposite membranes for water desalination, ACS Nano 7 (2013) 5308–5319.

[16] D. Emadzadeh, W. Lau, M. Rahbari-Sisakht, A. Daneshfar, M. Ghanbari, A. Mayahi, T. Matsuura, A. Ismail, A novel thin film nanocomposite reverse osmosis membrane with superior anti-organic fouling

affinity for water desalination, Desalination 368 (2015) 106–113.

[17] S. Roy, S.A. Ntim, S. Mitra, K.K. Sirkar, Facile fabrication of superior nanofiltration membranes from interfacially polymerized CNT-polymer composites, J. Membr. Sci. 375 (2011) 81–87.

[18] G.N.B. Baroña, J. Lim, M. Choi, B. Jung, Interfacial polymerization of polyamide-aluminosilicate SWNT nanocomposite membranes for reverse osmosis, Desalination 325 (2013) 138–147.

[19] W.-G. Kim, S. Nair, Membranes from nanoporous 1D and 2D materials: A review of opportunities, developments, and challenges, Chem. Eng. Sci. 104 (2013) 908–924.

[20] H. Huang, X. Qu, H. Dong, L. Zhang, H. Chen, Role of NaA zeolites in the interfacial polymerization process towards a polyamide nanocomposite reverse osmosis membrane, RSC Adv. 3 (2013) 8203.

[21] C. Kim, S. Kim, J. Lee, J. Kim, J. Yoon, Capacitive and oxidant generating properties of black-colored TiO_2 nanotube array fabricated by electrochemical self-doping, ACS Appl. Mater. Interfaces 7 (2015) 7486–7491.

[22] Y. Baek, J. Kang, P. Theato, J. Yoon, Measuring hydrophilicity of RO membranes by contact angles via sessile drop and captive bubble method: A comparative study, Desalination 303 (2012) 23–28.

[23] Y. Baek, J. Yu, S.-H. Kim, S. Lee, J. Yoon, Effect of surface properties of reverse osmosis membranes on biofouling occurrence under filtration conditions, J. Membr. Sci. 382 (2011) 91–99.

[24] J. Wijmans, R. Baker, The solution-diffusion model: A review, J. Membr. Sci. 107 (1995) 1–21.

[25] A.-H.M.A. El-Aassar, Improvement of reverse osmosis performance of polyamide thin-film composite membranes using TiO_2 nanoparticles, Desalin. Water Treat. 55 (2015) 2939–2950.